INSTITUTE OF PHYSICS PUBLISHING PHYSICS IN MEDICINE AND BIOLOGY

Phys. Med. Biol. **50** (2005) 2209–2224 doi:10.1088/0031-9155/50/10/002

A kinetic model for dynamic [^{18}F]-Fmiso PET data to analyse tumour hypoxia

Daniela Thorwarth[1], **Susanne M Eschmann**[2], **Frank Paulsen**[3] **and Markus Alber**[1]

[1] Section for Biomedical Physics, University Hospital for Radiation Oncology, Hoppe-Seyler-Str. 3, 72076 Tübingen, Germany
[2] Department of Nuclear Medicine, Radiological University Clinic, Otfried-Müller-Str. 14, 72076 Tübingen, Germany
[3] Department of Radiation Therapy, University Hospital for Radiation Oncology, Hoppe-Seyler-Str. 3, 72076 Tübingen, Germany

E-mail: daniela.thorwarth@med.uni-tuebingen.de

Received 22 November 2004, in final form 9 February 2005
Published 27 April 2005
Online at stacks.iop.org/PMB/50/2209

Abstract

A method is presented to identify and quantify hypoxia in human head-and-neck tumours based on dynamic [^{18}F]-Fmiso PET patient data, using a model for the tracer transport. A compartmental model was developed, inspired by recent immunohistochemical investigations with the tracer pimonidazole. In order to take the trapping of the tracer and the diffusion in interstitial space into account, the kinetic model consists of two compartments and a specific input function. This voxel-based data analysis allows us to decompose the time-activity curves (TACs) into their perfusion, diffusion and hypoxia-induced retention components. This characterization ranges from well perfused tumours over diffusion limited hypoxia to strong hypoxia and necrosis. The overall shape of the TAC and the model parameters may point at the structural architecture of the tissue sample. The model addresses the two main problems associated with hypoxia imaging with PET. Firstly, the hypoxic areas are spatially separated from well perfused vessels, causing long diffusion times of the tracer. Secondly, tracer uptake occurs only in viable hypoxic cells, which constitute only a small subpopulation in the presence of necrosis. The resulting parameters such as the concentration of hypoxic cells and the perfusion are displayed in parameter plots ('hypoxia map'). Quantification of hypoxia performed with the presented kinetic model is more reliable than a criterion based on static standardized uptake values (SUV) at an early timepoint, because severely hypoxic/necrotic tissues show low uptake and are thus overlooked by SUV threshold identification. The derived independent measures for perfusion and hypoxia may provide a basis for individually adapted treatment planning.

(Some figures in this article are in colour only in the electronic version)

1. Introduction

Hypoxia in tumours, as measured by polarographic Eppendorf pO_2 histographs, has been associated with poor treatment outcome and survival (Nordsmark *et al* 1996, 2000). Thus, to measure and quantify hypoxia may be beneficial for patient selection or treatment modification. Individually adapted treatment strategies to overcome this therapy resistance, such as ARCON (Kaanders *et al* 2002) or hypoxia dose painting (Alber *et al* 2003), appear necessary and promising.

There have been several attempts to quantify tumour hypoxia with polarographic needle electrodes (Nordsmark *et al* 1996, 2000) or with positron emission tomography (PET) by using hypoxia-specific tracer molecules such as [^{60}Cu]-ATSM (Chao *et al* 2001), [^{18}F]-Fluoroerythronitroimidazole (FETNIM) (Lehtiö *et al* 2004), [^{18}F]-Fluoroazomycin (FAZA) (Machulla 1999) or [^{18}F]-Fluoromisonidazole (Fmiso) (Koh *et al* 1992, Rasey *et al* 1996).

Fmiso binds selectively to macromolecules in hypoxic cells. At low oxygen levels, the compound is reduced and binds, when reduced by a second electron, covalently to intracellular macromolecules. In the presence of oxygen, the favoured reaction is the re-oxygenation to the less reactive parent compound which is freely diffusible and clears from tissue (Laubenbacher and Schwaiger 2000).

Koh *et al* (1992) and Rasey *et al* (1996) developed a strategy for the identification and quantification of hypoxic tumour areas on the basis of Fmiso PET images. They pointed out the necessity of very long (2–4 h) examination protocols because of the slow transport and reaction mechanisms of the tracer molecules. These investigators defined a fractional hypoxic tumour volume which is the proportion of the tumour area presenting a tumour-to-blood activity ratio $\geqslant 1.4$ at 2–3 h post injection (p.i.). Their results displayed a highly variable character of human tumour hypoxia among different tumours and also among regions within the same tumour. A study by Bentzen *et al* (2003) reports on an unclear correlation between Fmiso PET scans and direct oxygen measurements with polarographic needle electrodes.

Casciari *et al* (1995) developed a kinetic compartment model for the transport and metabolism of Fmiso. This model aims to determine the cellular Fmiso reaction rate constant from time-activity data, which is assumed to reflect the mean local oxygen concentration. It consists of four compartments with a high number of free parameters. Hence, a certain number of parameters have to be fixed to increase the robustness of the model. The model is a classical kinetic model where the different compartments co-exist in the same volume. This is problematic because it assumes homogeneous oxygen concentration which contradicts the observation of concentration gradients in a tissue.

Fortunately, the pattern of tracer accumulation in hypoxic tumours can be made visible by histological investigations with the related compound pimonidazole. Ljungkvist *et al* (2002) and Janssen *et al* (2002, 2004) investigated the structural architecture of hypoxic tumours with pimonidazole. These studies depict hypoxic islands interspersed throughout the tissue on length scales between 100 and 500 μm, located in regions far from blood vessels and including necrotic tissue. A 'hypoxia signal' on macroscopic length scales (size of PET voxels: $4 \times 4 \times 4.25$ mm^3) emerges from an irregular heterogeneous distribution of tracer accumulation on microscopic length scales.

The essential fact that hypoxia exists spatially separated and at any rate far from perfused vessels was not explicitly taken into account by Casciari *et al* (1995). Also, it becomes evident that the total sub-volume which traps the tracer is rather small. These observations are typical of the problem and serve to make the point that hypoxia-PET imaging with any arbitrary tracer is more ambiguous and intricate than with tracers with an active transport mechanism and

Table 1. Table of acquired image frames for each patient ($n = 16$).

Time p.i. (min)	0–2	2–4	4–15	15–60	120	180	240
Acquisition time	12 × 10 s	8 × 15 s	11 × 60 s	9 × 5 min	1 × 5 min	1 × 8–9 min	1 × 10–12 min
Patient no.							
1, 4	×	×	×	×	×	×	×
3, 5, 7, 9, 10, 12, 13, 15	×	×	×	–	×	–	×
8	×	×	×	–	×	×	×
11, 16	×	×	×	×	×	–	×
2, 14	×	×	×	3 × 5 min	×	–	×
6	×	×	×	5 × 5 min	×	–	×

higher reaction rates, such as FDG, and to justify that some model is required to interpret the images.

The immunohistochemical studies also revealed large inter- and intra-patient differences in regard to tumour tissue vasculature. Hypoxia is only a consequence of the irregular geometry of the tumour vasculature. Therefore, it is essential that the model for the transport of the tracer from the perfused vessels to the hypoxic cell is general enough to include both the irregular tumour geometry and the inter-individual tumour heterogeneity.

In the following, a method to quantify hypoxia in tumours based on dynamic [^{18}F]-Fmiso PET patient data is presented. The kinetic model assumes physical, purely diffusive transport of the tracer molecule to the hypoxic cell, where it is trapped according to the local oxygen tension. The application of the model to patient data time-activity curves (TACs) yields the local concentration of hypoxic sub-volumes in each tumour voxel, allowing us to display the results in a parameter plot ('hypoxia map').

2. Methods and materials

2.1. Patient data

The dynamic PET data in this study were obtained from patients with head-and-neck tumours who were examined with the following protocol: with the start of the image acquisition, a tracer activity of $A_0 \simeq 400$ MBq Fmiso was injected. For the first 15–60 min, the PET scanner (Advance, General Electric, Milwaukee, US) was running in dynamic acquisition mode which resulted in a total of 31–40 image frames. Additionally, two static images were taken for all patients 2 and 4 h p.i. and for a few patients also at 3 h p.i. Detailed information about time points and corresponding acquisition durations for each examined patient ($n = 16$) are summarized in table 1.

A decay correction for the decomposition of the radioactive ^{18}F was performed for all data sets. The raw PET data were stored in three separate data sets, one dynamic set consisting of 31 image frames and two static data sets with one frame each. In order to implement a pointwise hypoxia analysis, it was necessary to match these three data sets. The corresponding rigid body transformation matrix was calculated by applying a mutual information algorithm (Viola and Wells 1997). This matching procedure reached an accuracy $\leqslant 2$ mm in the region of the tumour and allowed us to determine a TAC for each voxel.

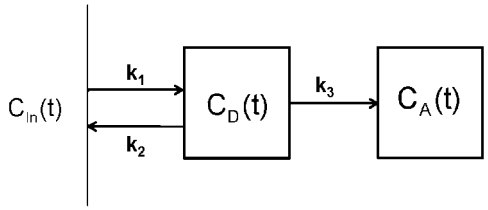

Figure 1. Compartmental model consisting of a diffusive and an accumulative compartment. The input function $C_{\mathrm{In}}(t)$ comprises the tracer concentration in the blood and in the interstitial space close to the vessels.

2.2. Kinetic model

Histochemical studies (Ljungkvist *et al* 2002, Janssen *et al* 2002, 2004) found increasing staining intensities for pimonidazole in addition to a larger quantity of cells accumulating the tracer molecules far from blood vessels. Typical distances for increased pimonidazole staining are 100–200 μm. Since there exists no active transport mechanism for pimonidazole or Fmiso in the interstitium, the transport of the tracer molecules is purely diffusive (Jain 1987). Considering the molecular weight of Fmiso and the distances the molecules have to travel from the vessel to the hypoxic cell (Jain 1987), the diffusion time will be high compared to other tracers with active transport mechanisms and shorter diffusion distances (such as e.g. FDG (Laubenbacher and Schwaiger *et al* 2000)). The time the marker needs to reach the hypoxic tissue area far from the blood vessel will be in the order of 100–1000 s, as motivated in the following.

Although the diffusive transport depends crucially on the tissue geometry, blood vessel permeability and the interstitial flow and pressure situation, which is obviously unknown, the bulk diffusion equation (without spatial dependences) for a net flow from a point A to a point B reads schematically:

$$\partial_t C_B = \frac{D}{l^2}(C_A(t) - C_B). \tag{1}$$

Here D is the diffusion constant, l the distance between points A and B and $C_A(t)$ is assumed to be unaffected by the efflux (infinite supply). The linearity of the diffusion equation allows us to associate spatially separated sub-volumes with compartments and an approximate linear reaction rate equation. For a compartmental model, the consequence of this diffusion delay will be a translation of the spatial separation of blood pool and tracer trapping into a temporal separation (Hicks *et al* 1997). With D typically in the order of 10^{-6} cm^2 s^{-1}, and $l \simeq 0.01$ cm it follows that $k \simeq 10^{-2}$ s^{-1}, i.e. typical time scales are >100 s.

Regarding the design of a kinetic model, it is assumed that for all practical purposes a general two compartment model (see figure 1) will be sufficient to describe the dynamic Fmiso data[4]. The model can be motivated by the heuristics that there are essentially three distinguishable components of the TACs. One, showing rapid concentration changes due to perfusion and fast diffusion into the interstitial space close to the vessels, represented by the input function. Another, characterized by slow concentration changes due to long diffusion times to and from the large inter-vessel spaces of irregular tumours. And a third, describing the irreversible binding of the tracer. In the following, the compartment describing the freely diffusive tracer molecules will be referred to as *diffusive* compartment. The *accumulative*

[4] This is a consequence of the integration of the manifold of various TACs of all the particular sub-volumes in a PET voxel. If tumours were more homogeneous or the spatial resolution of the scanner better, a chain of compartment pairs, stratified according to their diffusion time, might be a more appropriate model.

compartment is linked to the diffusive compartment by a kinetic rate constant that depends on the partial oxygen pressure.

In contrast to classic compartmental models, the compartments in this model are spatially separated or overlap only partially (the accumulative compartment corresponds only to those sub-volumes described by the diffusive compartment which are hypoxic) and the volumes of the different compartments are not identical. In addition, some of the kinetic constants of this model are not parameters of a chemical reaction, but reflect purely diffusive transport.

The diffusive compartment is linked to the input function by diffusion rate constants k_1 and k_2. The accumulative part is only coupled to the diffusive one with the rate constant k_3. It is assumed that the diffusion of unbound reduced Fmiso cannot be discerned on the time scales of the experiment. This kinetic model is described by the following system of differential equations:

$$\frac{\partial}{\partial t}C_D(t) = k_1 C_{\mathrm{In}}(t) - (k_2 + k_3)C_D(t) \tag{2}$$

$$\frac{\partial}{\partial t}C_A(t) = k_3 C_D(t). \tag{3}$$

$C_D(t)$ and $C_A(t)$ are the basis functions for the diffusive and the accumulative compartments respectively. They are determined by

$$\begin{aligned} C_D(t) &= \mathrm{e}^{-(k_2+k_3)t} \otimes k_1 C_{\mathrm{In}}(t) \\ &= k_1 \int_0^t \mathrm{e}^{-(k_2+k_3)(t-\tau)} C_{\mathrm{In}}(\tau)\,\mathrm{d}\tau \end{aligned} \tag{4}$$

and

$$\begin{aligned} C_A(t) &= k_3 \otimes C_D(t) \\ &= \frac{k_1 k_3}{k_2 + k_3} \int_0^t (1 - \mathrm{e}^{-(k_2+k_3)(t-\tau)}) C_{\mathrm{In}}(\tau)\,\mathrm{d}\tau, \end{aligned} \tag{5}$$

where the k_i are the respective rate constants and $\otimes$ denotes the convolution product. The total measured PET signal $S(t)$ is given by a linear combination of the basis functions (equations (4) and (5)) and the input function $C_{\mathrm{In}}(t)$:

$$\begin{aligned} S(t) &= w_0 C_{\mathrm{In}}(t) + w_D C_D(t) + w_A C_A(t) \\ &= w_0 C_{\mathrm{In}}(t) + w_D k_1 \int_0^t \mathrm{e}^{-(k_2+k_3)(t-\tau)} C_{\mathrm{In}}(\tau)\,\mathrm{d}\tau \\ &\quad + w_A \frac{k_1 k_3}{k_2 + k_3} \int_0^t (1 - \mathrm{e}^{-(k_2+k_3)(t-\tau)}) C_{\mathrm{In}}(\tau)\,\mathrm{d}\tau. \end{aligned} \tag{6}$$

Here w_D and w_A are the relative weights of the compartments. They represent the relative contribution of each compartment to the total signal. The weight parameters correspond, if properly normalized, to the volume fraction that is occupied by these compartments. Therefore, w_A could also be interpreted as the mean concentration of hypoxic cells in this voxel.

In the complete expression for the total signal $S(t)$ (equation (6)), the rate constant k_1 turns out to be only a multiplicative factor to the weight parameters w_D and w_A. It can therefore be set constant without loss of generality. Variations of this parameter are absorbed in $\tilde{w}_D = w_D k_1$ and $\tilde{w}_A$. Additionally, the rate constant k_2 can be absorbed by substituting $\tilde{k}_3 = k_2 + k_3$ and $\tilde{w}_A = w_A k_1 k_3 / \tilde{k}_3$. The final equation for the PET signal reads

$$S(t) = w_0 C_{\mathrm{In}}(t) + \tilde{w}_D \int_0^t \mathrm{e}^{-\tilde{k}_3(t-\tau)} C_{\mathrm{In}}(\tau)\,\mathrm{d}\tau + \tilde{w}_A \int_0^t (1 - \mathrm{e}^{-\tilde{k}_3(t-\tau)}) C_{\mathrm{In}}(\tau)\,\mathrm{d}\tau. \tag{7}$$

The remaining kinetic model has four open parameters, the weight parameters w_0, $\tilde{w}_D$ and $\tilde{w}_A$ in addition to the modified accumulation rate constant $\tilde{k}_3$.

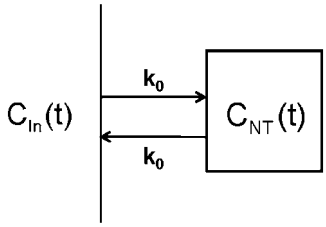

Figure 2. Reference tissue compartment.

2.3. Input function

For head and neck cases, it is difficult to obtain the blood input function directly from the images. Therefore, we propose the use of a reference tissue model. Normal tissues can be described by a kinetic model consisting of the blood concentration $C_{\mathrm{In}}(t)$ and a tightly coupled diffusive compartment, see figure 2. The tracer concentration in the cell layers around a blood vessel (i.e. the diffusive compartment of the normal tissue model) is denoted with $C_{\mathrm{NT}}(t)$. Therefore, the input function may be extracted from typical normal tissue voxels.

During the first minutes after injection, the image signal is governed by diffusion from well perfused capillaries into the interstitial space. This will occur in a similar fashion in both normal tissue and tumour tissue, although the deficient vasculature in tumours may offer less resistance. In this case, k_1 and k_2 of the tumour would be greater than in the reference tissue, but this does not affect the input function, which should be the same as long as the tracer transition from the vessel into the interstitial space is permeability limited and not flow limited. Apart from this difference in kinetic parameters, well perfused tumour areas and normal tissues should behave similarly during the first minutes after injection. This assumption is corroborated by immunohistochemical investigations (Ljungkvist *et al* 2002, Janssen *et al* 2002, 2004) that showed that cells situated in the neighbourhood of a blood vessel under well oxygenated conditions exist in both hypoxic and non-hypoxic tumours.

However, these investigations also show badly perfused vessels. Also, temporary stasis has been described in tumours (Denekamp and Daşu 1999). This means, that the well perfused vasculature which becomes visible in the first minutes after injection may not be the entire vasculature available for tracer transport by flow during the course of the investigation. Frequently, the distinction between chronic and acute hypoxia is made. The effect of fluctuations in the perfusion of a voxel on the TAC depends on the time scale of these fluctuations relative to the diffusion time scale, and the partial volume of the voxel affected by them. In our model, this is approximately taken into account by a spatially dependent input function as follows.

We assume, that the input function to the tumour kinetic model $C_{\mathrm{In}}(t)$ can be derived from the signal of a reference tissue $S_{\mathrm{NT}}(t) = AC_{\mathrm{In}}(t) + BC_{\mathrm{NT}}(t)$. We assume further that the blood concentration after a certain time after injection is a sum of two exponentials:

$$C_{\mathrm{In}} = \mathrm{e}^{-k_0 t} + r\,\mathrm{e}^{-k_K t}. \tag{8}$$

The first term $\mathrm{e}^{-k_0 t}$ describes the dispersion of the tracer in the whole body blood volume, whereas the second exponential represents the kidney clearance of the tracer. The rapid rise of tracer concentration in the blood pool observed in the very early frames is not taken into account by this input function. Therefore, the first frames (typically 4-5) have to be ignored for data analysis.

The concentration in the extravascular normal tissue space obtains from a convolution

$$C_{\mathrm{NT}}(t) = C_{\mathrm{In}}(t) \otimes \mathrm{e}^{-k_0 t}. \tag{9}$$

Here, we assume that the diffusion rate constant k_0 equals the mean rate of tracer flux into the extravascular volume, averaged over the whole body.

The signal measured in a reference tissue voxel $S_{\mathrm{NT}}(t)$ will be of the form

$$S_{\mathrm{NT}}(t) = A(\mathrm{e}^{-k_0 t} + r\,\mathrm{e}^{-k_K t}) + BC_{\mathrm{NT}}(t). \tag{10}$$

The parameters k_0 and k_K are determined by fitting this expression (equation (10)) to a set of TACs from a reference tissue in close proximity of the tumour. For the input function of a tumour voxel, these parameters are kept constant while r remains floating. This allows us to adapt the ratio between the fast and the slow component of the input function to the local properties of the tumour vasculature and perfusion, and to some extent to their temporal variability. The number of parameters in the fit of the voxel-by-voxel TACs to the compartment model (equation (7)) thereby increases to five.

2.4. Data evaluation

In order to evaluate the time-activity data with the presented kinetic model, a least-squares fit was performed to adjust the analytical function $S(t)$ (6) to the patient TACs. For this, a Levenberg–Marquardt algorithm was used (Press *et al* 1992).

The data points were included into the proximity function with errors corresponding to Poissonian noise. In analogy to Casciari *et al* (1995), standard deviations σ_i were calculated as scaled Poissonian noise, depending on local count rate $Y_i(t)$ and acquisition time T_i for the respective frame.

Additional uncertainties may occur due to image coregistration errors. As only the late data sets (2–4 h p.i.) undergo a matching procedure, additional errors have only to be taken into account for the late data points. The magnitude of the individual error associated with each image voxel depends strongly on the image gradient in the considered region. Hence, the error due to an eventual mismatch ΔY_{MM} can be estimated by

$$\Delta Y_{MM} = \Delta x \left(\sum_{i=1}^{n} \frac{(Y - Y_i)^2}{n x_i} \right)^{1/2}, \tag{11}$$

where Y_i are the count rates of the n neighbour voxels, x_i is the distance to the respective neighbour voxel and Δx represents the average coregistration error, which is assumed to be approximately 2 mm in our case. The total error associated with data points 2, 3 and 4 h p.i. is determined by $\Delta Y_i^{\mathrm{tot}} = \sigma_i Y_i + \Delta Y_{MM}$.

The variability of the model parameters due to the estimated data errors is then determined by the covariance matrix associated with the least-squares fit (Press *et al* 1992). The diagonal matrix elements represent estimates of the respective parameter variances.

In addition, the continuous automatic tracer injection during the first 10 s after the start of the acquisition is not taken into account by the model. To avoid problems, the very steep and slightly oscillating component dominating all data curves during the first 60 s was omitted.

In order to visualize the voxel-by-voxel results of the compartmental data analysis, *hypoxia maps* were generated by colouring each voxel of the tumour volume according to the tracer uptake at infinite times S_∞:

$$S_\infty = \lim_{t \to \infty} S(t) = \alpha \tilde{w}_A, \tag{12}$$

where $\alpha = Ak_1(1/k_0 + r/k_K)$. The parameter plots show areas presenting high levels of tracer uptake which correlates to the mean density of viable hypoxic cells in the respective voxel.

Prompted by the immunohistochemical experiments which imply that vascular density and hypoxia are independent parameters and which report a great variability of vascular geometries, a second visualization tool was devised. A *scatter plot* is generated by plotting the value of $w_A k_3$, describing the concentration of hypoxic cells weighted with the mean degree of hypoxia for each voxel on the abscissa against w_0 (the grade of perfusion) on the ordinate. Characteristic patterns in the scatter plots will allow us to distinguish between tumour areas according to vascular density and concentration of hypoxia.

3. Results

The TACs observed in a group of 16 examined patients showed great variability. In figure 3, four examples of characteristic shapes of the acquired time-activity data are displayed.

In well perfused regions[5], the shapes of the curves have a very pronounced tracer influx and distribution during the first few minutes after tracer injection followed by an exponential washout (see figure 3(a)). These tumour areas are characterized by a high density of vessels and a good blood supply. The majority of cells should be well oxygenated because no tracer retention can be seen.

In figure 3(b), a very similar behaviour can be observed during the first 30 min, followed by a clear retention. This shows that a large number of viable hypoxic cells are present, which co-exist with a very well perfused cell population. This is the classical picture of diffusion limited hypoxia, where oxygen consumption outweighs supply.

More serious forms of hypoxia result from a deficient vasculature and chaotic blood flow. However, this may also result in a decrease of viable hypoxic cells as necrotic cores may form in which no tracer retention occurs. In terms of the TAC, the perfusion peak should become smaller, and retention less pronounced until finally a horizontal curve type results, see figures 3(c) and (d). In voxels with a significant concentration of necrosis, the purely diffusive contribution to the signal as represented by w_D and r should go up. The tracer enters these tissue regions very slowly due to the low density of blood vessels. Accumulation of tracer can be observed in the order of several hours after injection (see figure 3(d)). Because of the small fraction of viable hypoxic cells, the total uptake is low.

Figure 4 shows the analytical curves $S(t)$ determined by the kinetic analysis for the data TACs presented in figure 3. The corresponding parameter values are summarized in table 2, whereas table 3 shows the corresponding parameter value uncertainties.

In summary, figures 3 (a)–(d) represent the TACs in tumour regions with increasingly deficient vasculature. The tracer influx peak at short timepoints after injection decreases as the blood supply gets worse due to the more and more chaotic vasculature. At the same time, while the number of viable hypoxic cells decreases (w_A), the degree of hypoxia increases (k_3). The kinetic analysis showed that the resulting parameter values might reveal information about the structural architecture of the tissue sample. Curve types representing putatively well perfused and only slightly hypoxic tumours (such as figure 4(a)) are described by a relatively high weight parameter w_0 in addition to a small value for the product $\tilde{w}_A \tilde{k}_3$ for the hypoxic compartment. Also for the diffusion limited hypoxia type (figure 4(b)) a large w_0 is found, but in this case the value of $\tilde{w}_A$ and thus S_∞ is also high.

In contrast, there exist tumour areas where very small parameters w_0 are necessary to describe the time-activity course of the data adequately. This behaviour is mainly observed

[5] Good perfusion/high vascular density is supposed in regions where the dynamic TAC presents a fast tracer influx after injection ($\approx$ 30–40 s).

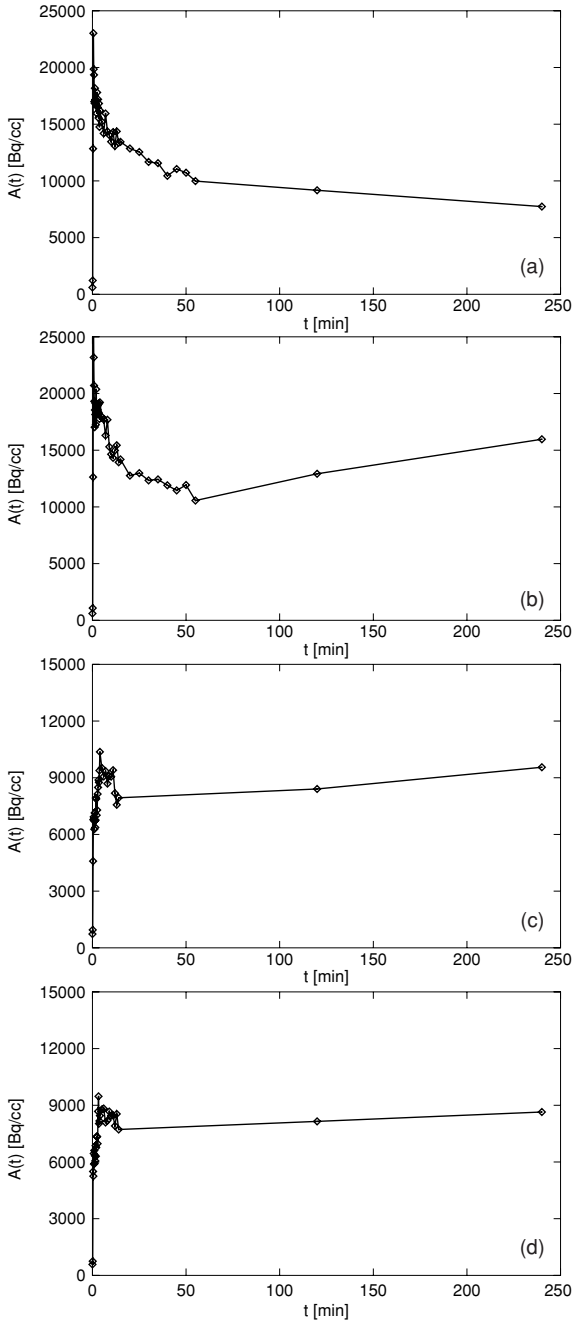

Figure 3. Different characteristic time-activity data curves corresponding to tumour areas with increasingly deficient vasculature. (a) Well perfused tumor area. (b) Tissue area with diffusion limited hypoxia. (c) Diffusion limited and structural hypoxia. (d) Hypoxic/necrotic area.

for curves that putatively represent severely hypoxic or necrotic tissues (such as figures 4(c) and (d)). Hence, $\tilde{w}_A\tilde{k}_3$ turns out to take relatively high values.

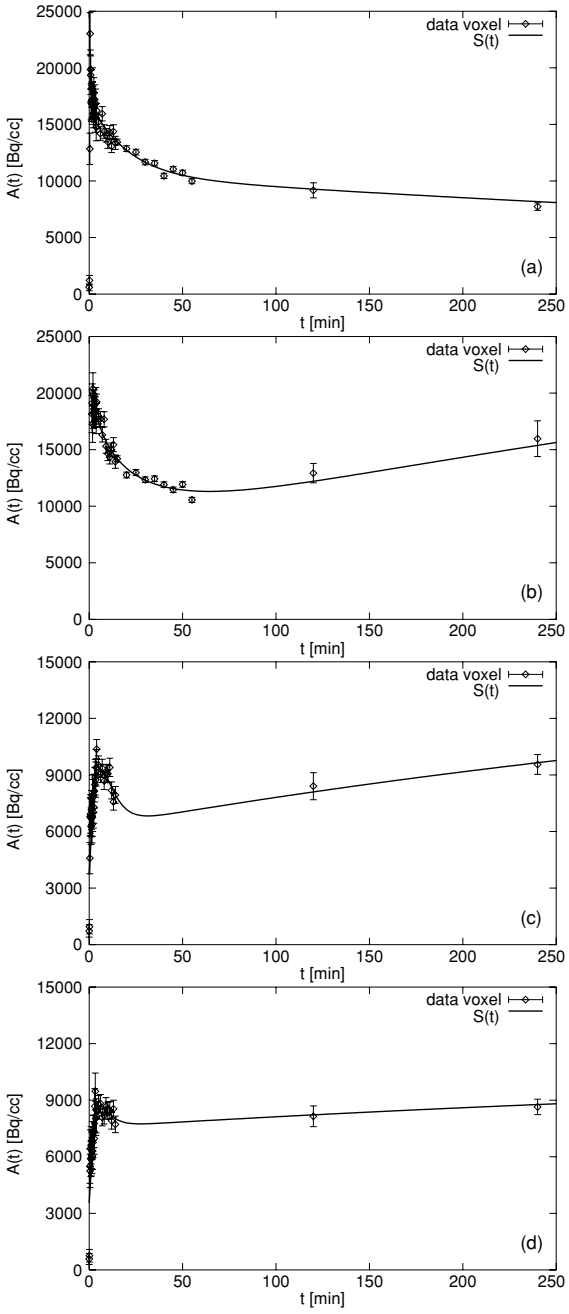

Figure 4. Resulting analytical time-activity curves corresponding to data curves (a)–(d) of figure 3.

In the following, the kinetic data analysis will be shown in more detail exemplarily for two of the 16 examined patients. Nevertheless, a kinetic analysis was performed for each data set, but they cannot all be shown in the context of this paper.

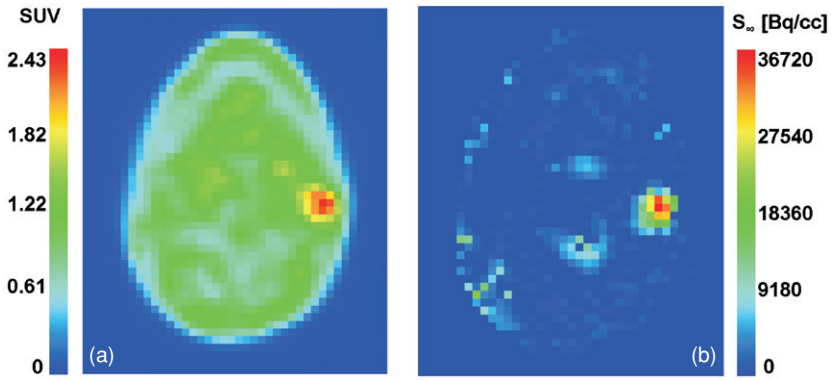

Figure 5. Tumour region of a head-and-neck patient: (a) SUV distribution 2 h p.i. for a whole PET slice, (b) parametric plot: S_∞ for each voxel.

Table 2. Resulting parameter values for curves (a)–(d), figure 4.

	Putative structure types	w_0	r	$\tilde{w}_D$ (min^{-1})	$\tilde{w}_A$ (min^{-1})	$\tilde{k}_3$ (min^{-1})
(a)	Low hypoxia/ well perfused	1.06	0.29	0.09	0.00	–
(b)	Diffusion limited hypoxia	1.50	0.10	0.13	0.31	0.03
(c)	Diffusion limited and structural hypoxia	0.32	0.45	0.28	0.08	0.21
(d)	Strongly hypoxic/ necrotic	0.16	1.67	0.14	0.01	0.36

Table 3. Errors of model parameters due to image noise and coregistration uncertainties associated with curves (a)–(d), figure 4.

	Δw_0	Δr	$\Delta\tilde{w}_D$ (min^{-1})	$\Delta\tilde{w}_A$ (min^{-1})	$\Delta\tilde{k}_3$ (min^{-1})
(a)	0.17	0.17	0.02	0.00	–
(b)	0.18	0.11	0.02	0.11	0.02
(c)	0.16	0.39	0.06	0.08	0.11
(d)	0.18	1.86	0.07	0.01	0.25

Figures 5(b) and 7(b) show S_∞ parameter plots of two different patients. Both hypoxia maps are displayed in comparison to the corresponding SUV distributions at 2 h p.i. (figures 5(a) and 7(a)).

Figure 5(b) represents a first example of a parametric plot for a head-and-neck patient. The region characterized by an increased SUV 2 h p.i. is also highlighted in the parametric plot. A typical TAC of this region is plotted in figure 6. The curve shows a relatively high influx peak as well as a positive slope for long times after injection.

In the second case, displayed in figure 7, the SUV image 2 h after injection indicates two distinct areas where the tracer seems to be accumulated (figure 7(a)). However, the parametric plot for the indicated region of interest only highlights one of these two regions (figure 7(b)). This phenomenon is due to a different overall shape of the curves in the respective tumour

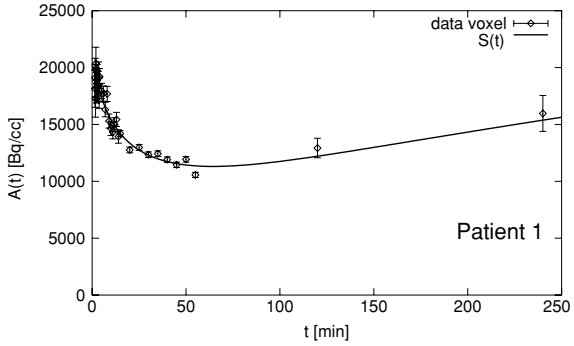

Figure 6. Typical TAC of the tracer accumulating region in figure 5.

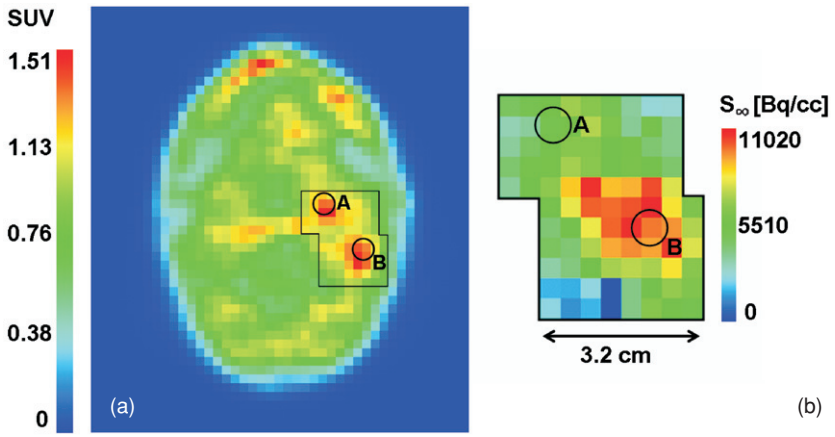

Figure 7. (a) SUV distribution 2 h p.i., (b) parametric plot for the marked tumour region: S_∞ for each voxel.

voxels and may be caused by different architectures of the tumour vascularization leading to different diffusion times for the tracer.

Voxels A and B were chosen as representatives for these two areas. The analytical curves $S(t)$ as well as the corresponding measured data points are displayed in figure 8. The plotted TACs present an interesting behaviour: even though the two curves have nearly the same activity level 120 min after tracer injection, the shape of the curves is completely different. While the TAC for voxel A shows a very high tracer influx peak followed by a continuous washout, voxel B is characterized by a steady accumulation of tracer 30 to 240 min p.i. in addition to a much lower influx peak at the beginning. Hence, the impression that the static image 2 h after injection presented the same level of tracer accumulation was due to the fact that the intercept point of two absolutely different curves was situated coincidentally at the time of image acquisition. Therefore, it does not seem reliable to identify hypoxia only on the basis of a static image 2 h p.i. which obviously bears high risks of incorrect interpretation.

An additional tool to analyse hypoxia and perfusion characteristics of a tumour is provided by the $(w_0, w_A k_3)$ scatter plot. It allows us to determine the dominating type of structural architecture in the tumour volume. Patients displaying large values for w_0 for most of the voxels have putatively well perfused tumours. Whereas, if the tumour contains hypoxic cores,

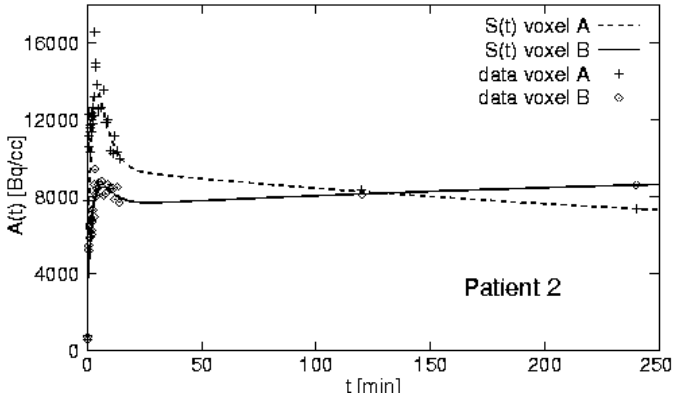

Figure 8. Comparison of the overall curve shapes of voxels *A* and *B*, figure 7.

the corresponding $w_A k_3$-parameters will have high values and will therefore be situated in the lower right area of the scatter plot. Hence, the presented scatter plot provides a medium to classify tumours according to different characteristic structure types.

For the two patients exemplarily shown above (figures 3 and 5), scatter plots have been generated. The analysis of the scatter plot for patient 1 (figure 9(a)) reveals that a large fraction of the tumour volume has relatively high levels of perfusion together with rather small concentrations of hypoxia. In contrast, patient 2 (figure 9(b)) shows for the whole tumour very low perfusion values, and at the same time high concentrations of hypoxia are observed.

4. Discussion

The presented investigation showed that the overall shapes of the TACs contain essential information about hypoxic tumour areas. Particularly the behaviour of the curves at long time scales is important. Hence, a criterion based on a single time point threshold is not sufficient to perform a reliable hypoxia analysis. The use of a static criterion to identify hypoxia in Fmiso PET scans might have been a reason why Bentzen *et al* (2003) could not find a clear correlation between PET and Eppendorf electrode measurements.

Curve features such as the position of the minimum in the TACs between 20 and 60 min hint at the characteristics of the underlying processes which occur on corresponding time scales. This property is understandable by the immunohistochemical investigations with pimonidazole (Ljungkvist *et al* 2002, Janssen *et al* 2002, 2004) that found that long diffusion distances had to be travelled by the tracer before reaching hypoxic cells. The signature of the characteristic diffusion times in the tumour tissue is the position of the minimum in the curves.

Different tumour structure types may be associated with different characteristic shapes of the TACs. Putatively well perfused and regularly vascularized tumours show curves with a high influx peak and exponential washout, whereas a good perfusion together with diffusion limited hypoxia should result in a positive slope at long time scales, leading to high tracer uptake values S_∞. The curves probably corresponding to severely hypoxic or necrotic tissues present no influx peak and a horizontal time trend remaining at relatively low SUV levels. These results can be understood by comparison with the microscopic tissue sections presented by other investigators (Ljungkvist *et al* 2002), where different characteristic hypoxia patterns (‘patchy’ and ‘ribbon-like’) were found.

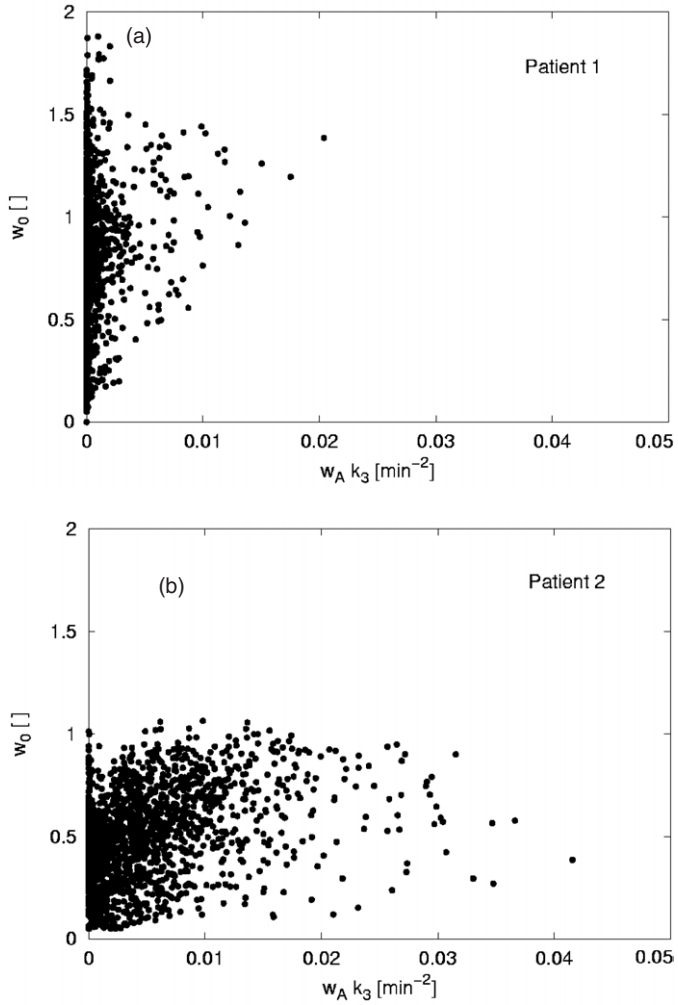

Figure 9. Scatter plots for two patients. (a) Patient 1 (cf figure 3) shows a quite well perfused and only moderately hypoxic tumour. (b) Patient 2 (cf figure 5) in contrast has a badly perfused and severely hypoxic tumour.

A particular problem with severely hypoxic areas is the presence of necrosis. Since Fmiso uptake occurs only in viable hypoxic cells, a low uptake may be caused by a small fraction of surviving cells. This is compounded by the finding that the binding rate constant is similar to the rate of renal clearance, so that the net effect can be a constant signal. In contrast, tumour areas that present very high levels of tracer uptake consist of many viable, hypoxic cells by necessity. These may not be the most resistant tumours and they might constitute a group that highly benefits from individually adapted therapies. A classification of the patients according to these criteria can be performed on the basis of the introduced perfusion-hypoxia scatter plots.

The presented model involves slow diffusion rates of the tracer in the interstitium, caused by long diffusion distances in the tumour tissue. It also respects the inherent heterogeneity of tumour tissues, where well perfused and hypoxic sub-volumes may coexist in the same

PET voxel. These facts were not considered by previous models (Casciari *et al* 1995), which explicitly treated homogeneous tumour tissues and were more appropriate to normal tissues made hypoxic under experimental conditions.

The heterogeneity of the tumour structure requires that all compartment weights remain floating in the fits to accommodate partial volume effects by virtue of the linearity of the differential equation and the input function becomes spatially variable. Due to the particular choice of the input function and the assumption of physical transport into the diffusive compartment which ensures $k_{1,\mathrm{in}} = k_{1,\mathrm{out}}$, the total number of fit parameters is five. This reduces the variability and co-variance of the fits. The experimentally established need for a spatially variable input function poses an obstacle to the use of graphical TAC analysis.

5. Conclusion

The investigated method allows us to identify and quantify hypoxia in human head-and-neck tumours based on dynamic Fmiso PET scans better than SUV alone. Hypoxia is essentially a consequence of irregular vascularization, and this needs to be taken into account when time-activity curves of hypoxia PET tracers are interpreted. Perfusion and the degree of hypoxia seem to be independent properties of a tumour.

Acknowledgments

We would like to thank Professor H-J Machulla (Department of Radiopharmacy, University Hospital Tübingen) and his team for [^{18}F]-Fmiso tracer production. We also thank Professor A van der Kogel and Dr A Ljungkvist (University Medical Center Nijmegen, The Netherlands) and Professor A Begg (The Netherlands Cancer Institute, Amsterdam, The Netherlands) for helpful discussions.

This project was financially supported by the *f*ortüne program of the University Hospital Tübingen, grant no. 1161-0-0 and by the German Research Foundation (DFG), grant no. AL 877/1-1.

References

Alber M, Paulsen F, Eschmann S M and Machulla H-J 2003 On biologically conformal boost dose optimization *Phys. Med. Biol.* **48** N31–5

Bentzen L, Keiding S, Nordsmark M, Falborg L, Hansen S B, Keller J, Nielsen O S and Overgaard J 2003 Tumour oxygenation assessed by ^{18}F-fluoromisonidazole PET and polarographic needle electrodes in human soft tissue tumours *Radiother. Oncol.* **67** 339–44

Casciari J J, Graham M M and Rasey J S 1995 A modeling approach for quantifying tumor hypoxia with [F-18]fluoromisonidazole PET time-activity data *Med. Phys.* **22** 1127–39

Chao K S C, Bosch W R, Mutic S, Lewis J S, Dehdashti F, Mintun J F, Dempsey J F, Perez C A, Purdy J A and Welch M J 2001 A novel approach to overcome hypoxic tumor resistance: cu-aTSM-guided intensity-modulated radiation therapy *Int. J. Radiat. Oncol. Biol. Phys.* **49** 1171–82

Denekamp J and Daşu A 1999 Inducible repair and the two forms of tumour hypoxia—time for a paradigm shift *Acta Oncol.* **38** 903–18

Hicks K O, Ohms S J, van Zijl P L, Denny W A, Hunter P J and Wilson W R 1997 An experimental and mathematical model for the extravascular transport of a DNA intercalator in tumours *Br. J. Cancer* **76** 894–903

Jain R K 1987 Transport of molecules in the tumor interstitium: a review *Cancer Res.* **47** 3039–51

Janssen H L K *et al* 2002 HIF-1A, pimonidazole, and iododeoxyuridine to estimate hypoxia and perfusion in human head-and-neck tumors *Int. J. Radiat. Oncol. Biol. Phys.* **54** 1537–49

Janssen H L K, Hoebers F J, Sprong D, Goethals L, Williams K J, Stratford I J, Haustermans K M, Balm A J and Begg A C 2004 Differentiation-associated staining with anti-pimonidazole antibodies in head and neck tumors *Radiother. Oncol.* **70** 91–7

Kaanders J H A M, Bussink J and van der Kogel A J 2002 ARCON: a novel biology-based approach in radiotherapy *Lancet Oncol*. **3** 728–37

Koh W-J, Rasey J S, Evans M L, Grierson J R, Lewellen T K, Graham M M, Krohn K A and Griffin T W 1992 Imaging of hypoxia in human tumors with [F-18]fluoromisonidazole *Int. J. Radiat. Oncol. Biol. Phys*. **22** 199–212

Laubenbacher C and Schwaiger M 2000 The potential role of positron emission tomography in investigation of microenvironment *Blood Perfusion and Microenvironment of Human Tumors* ed M Molls and P Vaupel (Berlin: Springer)

Lehtiö K, Eskola O, Viljanen T, Oikonen V, Grönroos T, Sillanmäki L, Grénman R and Minn H 2004 Imaging perfusion and hypoxia with PET to predict radiotherapy response in head-and-neck cancer *Int. J. Radiat. Oncol. Biol. Phys*. **59** 971-82

Ljungkvist A S E, Bussink J, Rijken P F J W, Kaanders J H A M, van der Kogel A J and Denekamp J 2002 Vascular architecture, hypoxia, and proliferation in first-generation xenografts of human head-and-neck squamous cell carcinomas *Int. J. Radiat. Oncol. Biol. Phys*. **54** 215–28

Machulla H-J 1999 *Imaging of Hypoxia* (Dordrecht: Kluwer)

Nordsmark M and Overgaard J 2000 A confirmatory prognostic study on oxygenation status and loco-regional control in advanced head and neck squamous cell carcinoma treated by radiation therapy *Radiother. Oncol*. **57** 39–43

Nordsmark M, Overgaard M and Overgaard J 1996 Pretreatment oxygenation predicts radiation response in advanced squamous cell carcinoma of the head and neck *Radiother. Oncol*. **41** 31–9

Press W H, Teukolsky S A, Vetterling W T and Flannery B P 1992 *Numerical Recipes in C: The Art of Scientific Computing* 2nd edn (Cambridge: Cambridge University Press)

Rasey J S, Koh W-J, Evans M L, Peterson L M, Lewellen T K, Graham M M and Krohn K A 1996 Quantifying regional hypoxia in human tumors with positron emission tomography of [^{1}8F]fluoromisonidazole: a pretherapy study of 37 patients *Int. J. Radiat. Oncol. Biol. Phys*. **36** 417–28

Viola P and Wells W M 1997 Alignment by maximization of mutual information *Int. J. Comput. Vis*. **24** 137–54